MEMS for Plasmon Control of Optical Metamaterials

Yoshiaki Kanamori, Ryohei Hokari, and Kazuhiro Hane

(Invited Paper)

***Abstract*—Metamaterials have attracted a great deal of attention as artificial electromagnetic materials having unique optical characteristics, and various innovative optical applications have been expected. Micro electromechanical systems (MEMS)-based reconfigurable metamaterials are candidate technologies for active optical control. In this paper, we focus on MEMS-based reconfigurable metamaterials operated in the optical region between visible and near-infrared wavelengths. A brief overview of static optical metamaterials and active optical metamaterials driven by MEMS actuators is presented. Moreover, points to be considered for a micromachining process of optical metamaterials are discussed with results of calculations.**

***Index Terms*—Microelectromechanical systems, microfabrication, nanophotonics, optical metamaterials, plasmons.**

I. Introduction

METAMATERIALS with unit structures smaller than operation wavelengths have attracted a great deal of attention as artificial electromagnetic materials having unique optical characteristics including a negative refractive index [1]–[4] and a high refractive index [5], [6], which does not exist in nature.

Since a wide range of refractive indices from negative to positive values can be obtained by metamaterials, a variety of innovative optical applications have been expected and the number of publications on investigations of metamaterials has been increasing yearly. The most popular application of metamaterials described in past publications is antennas. Study of negative refraction and applications to sensors, acoustic devices, and absorbers have been frequently reported. Super lenses [2], [7]–[11], cloaking devices [12], [13], solar cells [14], [15], and optical storages [16], [17] are candidate applications of metamaterials. Applications of metamaterials for sensors were summarized by Chen *et al*. [18]. Biosensors [19]–[21], thin-film sensors [22]–[24], strain sensors [25], [26], and other sensors have been under intense investigation.

Metamaterials have often been compared directly with photonic crystals. Negative refraction in photonic crystals has also been demonstrated in the optical region [27]. However, photonic crystals have periodic structures with the periods close to operation wavelengths. The optical resolution is therefore limited by the structural size. On the other hand, since metamaterials have smaller sizes than operation wavelengths and can work as a unit structure, realization of ultimate small devices and truly effective and artificial optical materials with good control of the distribution of refractive indices have been expected. Based on the novel concept in which permittivity and permeability in space can be controlled by metamaterials, a new field called transformation optics [27]–[29] has been developed and adapted to the design of cloaking devices [29], concentrators [30], and waveguides [31].

In order to control the optical properties of metamaterials at an operation wavelength, metamaterials are mostly designed to have optical resonant structures and operate at a certain wavelength that depends on a resonant wavelength. Active optical control by metamaterials, enabling tuning, modulating, and switching at resonant wavelengths, has recently attracted attention [32]–[34]. To realize this goal, studies on tunable metamaterials have been carried out using various methods including electrical controls utilizing semiconductors [35]–[40], magnetostatic control [41], optical controls [42]–[45], phase-change media [46]–[49], liquid crystals [50], [51], and mechanical controls utilizing micro electromechanical systems (MEMS) [52]–[61]. Active optical devices having unprecedented optical characteristics have been realized by using tunable metamaterials. In the microwave and terahertz regions, since the fabrication is relatively easy, several devices have been reported. For example, Chen *et al*. reported electrically tunable metamaterials for a phase shifter [36]. Transmittance at 0.81 THz was changed from 56% to 25% by a change in applied voltage from 0 to 16 V. The phase of transmission at 0.89 THz was shifted from 0.05 to -0.51 radians by a change in applied voltage from 0 to 16 V. For the use of MEMS actuators, Zhu *et al*. demonstrated switchable magnetic metamaterials [52]. The metamaterial molecules consisted of two semi-square split rings. The gap between the split rings could be controlled by a MEMS actuator and thus optical response of the metamaterial molecules could be changed. The resonant frequency was shifted from about 2 to 2.5 THz.

Although there is not a strict definition, metamaterials having operating wavelengths from the visible to near-infrared region are called optical metamaterials. Since structural dimensions of optical metamaterials from tens of nanometers to hundreds of nanometers are required, precise fabrication of the metamaterials is a difficult process. Moreover, since the real part of the relative permittivity of metals, such as silver, gold, copper, and aluminum, gradually approaches from negative to zero with decrease in wavelengths because of the wavelength approaching the plasma frequency and electronic interband transitions of metals, these metals gradually lose optical characteristics as metals. Hence, it is necessary to pay attention to the optical dispersion of constructional materials for metamaterials.

In the optical region, the tuning method for the use of semiconductors is limited by the material properties of semicon-

Manuscript received October 11, 2014; revised December 11, 2014 and December 16, 2014; accepted December 17, 2014. Date of publication January 21, 2015; date of current version January 27, 2015. This work was supported by MEXT KAKENHI 25109702.

The authors are with the Department of Nanomechanics, Tohoku University, Sendai 980-8579, Japan (e-mail: kanamori@hane.mech.tohoku.ac.jp; hokari@hane.mech.tohoku.ac.jp; hane2@hane.mech.tohoku.ac.jp).

Color versions of one or more of the figures in this paper are available online at http://ieeexplore.ieee.org.

Digital Object Identifier 10.1109/JSTQE.2014.2385957

ductors. Even if a carrier is injected into the semiconductor, the carrier density is not sufficient for operation at optical frequencies. On the other hand, optical characteristics of metamaterials depend on the shape of the structure, which is independent of operation frequencies. Therefore, mechanically reconfigurable metamaterials integrated with MEMS actuators have the potential to provide a wide range of controllability of the metamaterial properties in the optical region. MEMS technology is widely used for tuning, modulating, and switching a variety of optical devices such as optical sensors, optical filters, optical scanners, and optical switches. In addition, mechanically reconfigurable metamaterials can be operated at a small actuation force, high response speed, and low power consumption because the mechanical motion required for their motion is considerably smaller than that for conventional MEMS applications. Although there have been several reports on mechanically reconfigurable metamaterials in the microwave and terahertz regions [52]–[58], there have been few reports on these metamaterials in the optical region [59]–[61].

In this paper, plasmon control of optical metamaterials with focus on MEMS-based reconfigurable optical metamaterials is discussed. In Section II, a brief overview of static optical metamaterials in terms of optical characteristics and classification of structures is given. In Section III, characteristics of MEMS-based reconfigurable optical metamaterials are described and previous studies are discussed. In Section IV, important points for optical metamaterials fabricated by a micromachining process are discussed with results of calculations.

II. Static Optical Metamaterials

Stationary optical metamaterials have been extensively studied. Although the optical design of metamaterials in the optical region is difficult because of Joule loss of the constructional material of metamaterials, several types of metamaterial structures that produce excellent magnetic responses have been proposed. If these types of metamaterial structures can be integrated with MEMS actuators, realization of active and applicable metamaterial devices with widely tunable characteristics is expected. In this section, selection of constructional materials for optical metamaterials and typical structures producing excellent magnetic responses at optical wavelengths are discussed.

A. Selection of Constructional Materials for Optical Metamaterials

Conventionally, usage of metals in optical systems is limited to only a few applications such as mirrors and optical thin films [62]. In optical metamaterials, however, usage of metals is essential for obtaining newfangled optical responses as metamaterials. There are several models to understand the optical properties of metals [63]–[66]. In general, the free-electron Drude model is not adequate in the near-infrared and visible wavelength regions due to the interband effects. Here, we introduce the Lorentz-Drude oscillator model [63], [66]. For parameterization of the permittivity of metals, the complex permittivity ε_r as a function of frequency ω is expressed by the following equation:

$$\varepsilon_r(\omega) = \varepsilon_{rf}(\omega) + \varepsilon_{rb}(\omega) \tag{1}$$

TABLE I
Plasma Frequency ω_p, Damping Constant Γ, and Fermi Velocity v_F of Selected Noble Metals [62]

Metal	$\omega_p\,(10^{15}/s)$	$\Gamma(10^{15}/s)$	$v_F\,(10^6 m/s)$
Silver	14.0	0.032	1.4
Gold	13.8	0.11	1.4
Copper	13.4	0.14	1.6
Aluminum	22.9	0.92	2.0

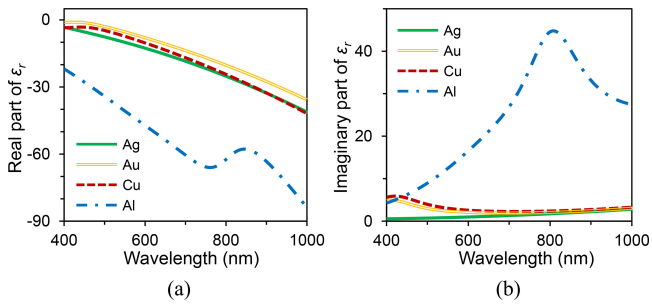

Fig. 1. Relative permittivity of silver, gold, copper, and aluminum. (a) The real part and (b) the imaginary part of the permittivity.

which separates the intraband effects from the interband effects. ε_{rf} and ε_{rb} are the intraband part and the interband part of the permittivity, respectively. The intraband effects and interband effects are usually referred to as free-electron effects and bound-electron effects, respectively. The intraband part ε_{rf} of the permittivity is described by the Drude model:

$$\varepsilon_{rf}(\omega) = 1 - \frac{f_0\omega_p^2}{\omega^2 + i\Gamma\omega} = 1 - \frac{f_0\omega_p^2}{\omega^2 + \Gamma^2} + i\frac{f_0\omega_p^2\Gamma}{\omega(\omega^2 + \Gamma^2)} \tag{2}$$

where ω_p is the volume plasma frequency, f_0 is the oscillator strength, and Γ is the damping constant. ω_p and Γ are expressed by the following equations:

$$\omega_p^2 = \sqrt{\frac{Ne^2}{\varepsilon_0 m}} \tag{3}$$

$$\Gamma = \frac{\nu_F}{l}, \tag{4}$$

where N is the density of free-electrons, e is the charge of an electron, ε_0 is permittivity of vacuum, m is mass of electrons, v_F is the Fermi velocity, and l is electron mean free path. Table I shows ω_p, Γ, and v_F of selected noble metals [62].

The interband part ε_{rb} of the permittivity is described by the simple semiquantum model resembling the Lorentz result for dielectrics [66]:

$$\varepsilon_{rb}(\omega) = \sum_{j=1}^{k} \frac{f_j\omega_p^2}{(\omega_j^2 - \omega^2) + i\omega\Gamma_j} \tag{5}$$

where k is the number of oscillators with frequency ω_j, strength f_j, and lifetime $1/\Gamma_j$. ω_j, f_j and Γ_j are listed in Ref. [66]. Fig. 1 shows the relative permittivity of silver, gold, copper, and aluminum according to Ref. [66]. It can be seen that ε_r shows different values depending on the materials. Therefore,

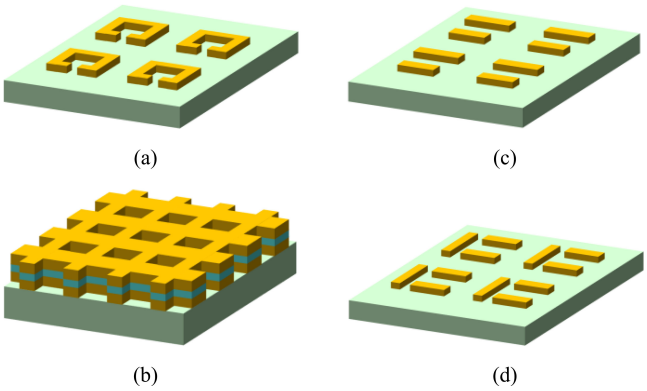

Fig. 2. Typical structures of optical metamaterials. (a) SRRs, (b) a fishnet structure, (c) plasmonic structures with Fano resonances, and (d) EIT metamaterials.

choosing a material suitable for each operating wavelength-band is important in order to obtain excellent characteristics of metamaterials in the optical region.

B. Typical Structures

Structures of optical metamaterials currently attracting attention include, for example, split ring resonators (SRRs) [67]–[72], fishnet structures [4], [73], [74], plasmonic structures (PSs) with Fano resonances [75]–[79], and electromagnetically induced transparency (EIT) metamaterials [80]–[88]. Typical structures of optical metamaterials are shown in Fig. 2.

Valentine *et al*. fabricated a fishnet structure with a negative refractive index at near-infrared wavelengths [4]. The structure consisted of metal-dielectric-metal layers (21 layers). Since relatively high transmittance with a negative refractive index is obtained, the fishnet structure provides much flexibility in optical design.

Shao *et al*. demonstrated PSs with Fano resonance [78]. They reported results of their investigation of plasmon coupling in heterodimers made of a large Au nano-rod and a small Au nano-sphere with the nano-sphere being located at different positions on the nano-rod surface. Fano dips were observed at wavelengths around 654 nm. Recently, Moritake *et al*. experimentally demonstrated Fano resonance in metamaterials composed of asymmetric double bars (ADBs), as schematically shown in Fig. 2(c), in the optical region [79]. Around a wavelength of 1100 nm, optical spectra clearly showed sharp Fano resonance. Because the structure of an ADB has asymmetry, a quadrupole mode with small radiative loss can be excited by a free-space electromagnetic wave. Thus, high Q-factor resonance can be obtained in the optical region.

An SRR is well known as the most representative structure in metamaterials. In the microwave region, a double SRR is mainly used as an SRR. In the optical region, however, a simple structure such as a single SRR or a U-shaped SRR is used as an SRR. Although the shapes are different for the microwave and optical regions, the basic principle of the operation is the same. In general, SRRs play a role in LC resonant circuits [67]. Solid structures and air gaps in SRRs correspond to a coil and a capacitor, respectively. The electromagnetic induction generated in SRRs by an incident magnetic field or an electric field makes a charge distribution. As a result, resonance occurs in the SRRs at a certain wavelength. Liu *et al*. fabricated four-layer SRRs consisting of U-shaped structures operating at near-infrared wavelengths [71]. Dimensions of the SRR were 80 nm in width, 380 nm in length in the vertical direction, and 430 nm in length in the horizontal direction. In the polarization directions parallel to the horizontal directions, the U-shaped SRR was resonated like the single SRR. Xu *et al*. reported U-shaped SRRs operating between visible and near-infrared wavelengths [72]. They observed resonance of the SRRs made of silver and gold at visible wavelengths. For silver SRRs of 30 nm in width and 30 nm in thickness, electric resonance at wavelengths of about 542 nm and magnetic resonance at wavelengths of about 756 nm were obtained.

EIT metamaterials generate an EIT-like effect in plasmonic circuits, based on the coupling between bright and dark modes arising from surface plasmon polariton [80]. They can suppress radiative losses over narrow spectrum regions due to a quantum interference effect in addition to playing a role in slow-light media and phase shifters because of drastic modifications of the dispersive properties. Moreover, since EIT-like effects are regulated by a change in the coupling efficiency between the two modes, the dispersive properties can be controlled according to the coupling efficiency. Liu *et al*. reported stacked EIT metamaterials having EIT-like effects at a frequency of 173 THz, which is 1733 nm in wavelength [81]. Verellen *et al*. observed EIT-like effects in gold metamaterials consisting of monomers and dimers at wavelengths around 780 nm [82]. Recently, Hokari *et al*. successfully demonstrated planar EIT metamaterials operating at the visible wavelengths of 462, 514, and 647 nm [88].

III. MEMS-Based Reconfigurable Optical Metamaterials

Even if there are stationary optical metamaterials with excellent optical characteristics, there exist difficult cases to simply integrate them with MEMS actuators for the reason of particular points that should be considered for MEMS-based reconfigurable metamaterial devices. In this section, characteristics of reconfigurable optical metamaterials are discussed and previous works on MEMS-based reconfigurable optical metamaterials are reviewed.

A. Characteristics of Reconfigurable Optical Metamaterials

1) Fundamental Principle of Active Metamaterials: Active metamaterials based on several tuning methods have been proposed. By using electron injection, optical excitation, thermal, and liquid crystal control, the refractive index of media can be tuned. If PSs are proximally positioned and surrounded by refractive-index-change media as shown in Fig. 3(a), coupling efficiency between the PSs can be controlled from $\eta_{\rm sp}$ to $\eta_{\rm sp} + \Delta\eta_{\rm sp}$ by changing the refractive index from N to $N + \Delta N$ as shown in Fig. 3(b). However, since the change in refractive index ΔN is very small, tuning range of the active metamaterials is limited to a relatively narrow range. MEMS is also one of the strong candidates for a tuning method. Unlike the tuning method mentioned above, by changing the position of PSs from L to $L + \Delta L$ using MEMS, coupling efficiency between the PSs can be controlled from $\eta_{\rm sp}$ to $\eta_{\rm sp} + \Delta\eta_{\rm sp}$ as shown in Fig. 4. When the distance between PSs is larger than several hundred

Fig. 3. Control of coupling efficiency via surface plasmon based on refractive index change of surrounding media. (a) Initial state and (b) active state.

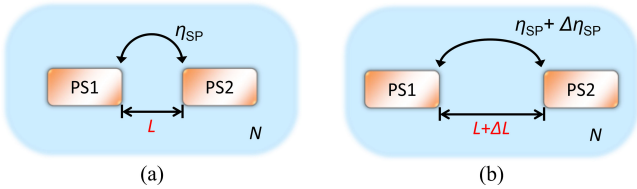

Fig. 4. Control of coupling efficiency via surface plasmon based on positioning change of plasmonic structures. (a) Initial state and (b) active state.

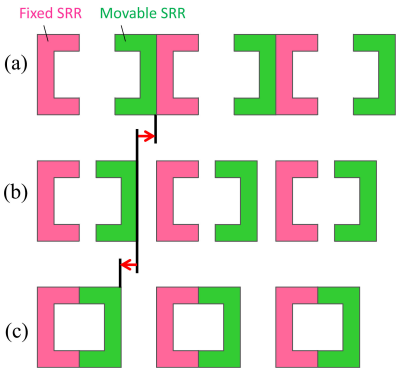

Fig. 5. Shape transformation of reconfigurable metamaterials. (a) "I" shape (back-touch state), (b) "[]" shape (open-ring state), and (c) "□" shape (closed-ring state).

nanometers, coupling of surface plasmons does not occur. Thus, control of the coupling efficiency from critical coupling to no coupling can be realized only in the position change of several hundred nanometers. Using MEMS technologies, metamaterial structures are controlled not only by a change in distance between the PSs but also by transformation of their shapes. Fig. 5 shows one example of shape transformation of metamaterials proposed by Zhu *et al*. [52]. The structure consists of an array of two SRRs in a face-to-face physical relationship with several gaps initially as shown in Fig. 5(b). One SRR is fixed and the other is movable. By controlling the position of the movable SRR, the shape of the unit structure can be transformed to an "I" shape (back-touch state), "[]" shape (open-ring state), and "□" shape (closed-ring state) as shown in Fig. 5(a), (b), and (c), respectively. Using MEMS actuators, Zhu *et al*. demonstrated structural transformation at THz wavelengths [52]. The resonant frequency was shifted from about 2 to 2.5 THz by a change in the gap between the two SRRs.

2) Particular Consideration for MEMS-Based Reconfigurable Optical Metamaterials: Fig. 6(a) shows the simplest configuration of reconfigurable optical metamaterials consisting of proximally positioned PS1 and PS2 which are located in media with

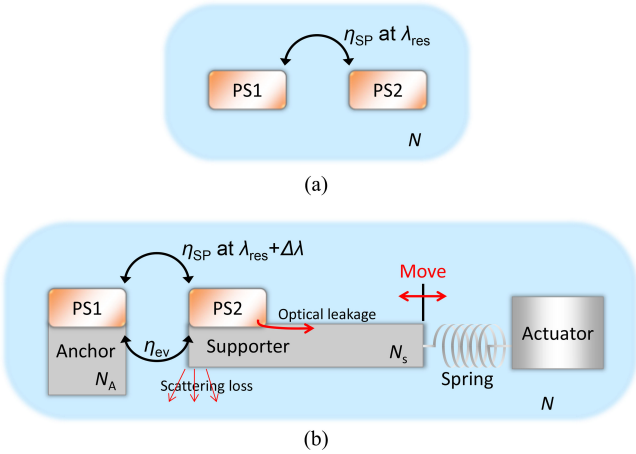

Fig. 6. Control of coupling efficiency between PS1 and PS2 via surface plasmon. (a) The simplest configuration adaptable to actual stationary optical metamaterials and (b) actual configuration of MEMS-based reconfigurable optical metamaterials.

a refractive index N. At a resonant wavelength $\lambda_{\rm res}$, the mode of the electromagnetic wave is coupled with metamaterials in which PS1 and PS2 are coupled via surface plasmon with a coupling efficiency $\eta_{\rm sp}$. In the case of stationary optical metamaterials, PSs are embedded in media such as air and a polymer or located on a low-refractive-index substrate such as glass. A schematic diagram of the optical system as shown in Fig. 6(a) is adaptable to actual stationary optical metamaterials. On the other hand, in the case of MEMS-based reconfigurable optical metamaterials as shown in Fig. 6(b), the fixed PS (PS1) is supported by an anchor and the movable PS (PS2) is formed on a supporter with refractive indices of $N_{\rm A}$ and $N_{\rm s}$, respectively. Si and Si_3N_4 are frequently used as materials of the anchor and supporter for MEMS structures because of their mechanical reliability. However, since Si and Si_3N_4 are high-refractive-index materials, they potentially influence optical characteristics in the shift of resonant wavelengths $\Delta\lambda$, unnecessary optical couplings between the anchor and supporter via evanescent fields with a coupling efficiency $\eta_{\rm ev}$, scattering losses, and optical leakage to the high-refractive-index materials, as shown in Fig. 6(b).

Adhesion of metamaterials to substrates is one of the particular considerations for fabrication of MEMS-based reconfigurable optical metamaterials. If the metamaterial parts are fabricated first, they need to be adhered tightly during the fabrication of MEMS parts. If the MEMS parts are fabricated first, on the other hand, metamaterial parts need to be formed on patterned indented surfaces of the MEMS structures. From another perspective, since metamaterials are mechanically moved repeatedly, peeling of metamaterials caused by cyclic stress and strain might occur in the case of weak adhesion.

B. Previous Works

In 2010, Pryce *et al*. demonstrated stretchable metamaterials formed on flexible substrates as shown in Fig. 7 [59]. Unit structures consisting of a U-shaped structure and a straight bar with a gap between them were arrayed. By stretching the flexible substrate consisting of polydimethylsiloxane (PDMS), the gap was changed and then the resonant wavelength was tuned. The reso-

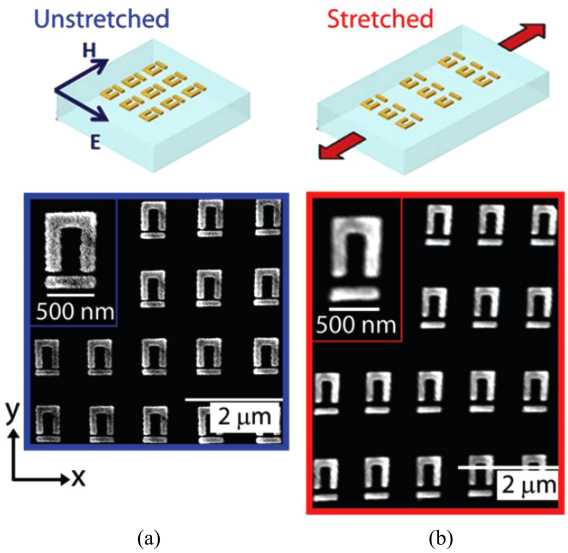

Fig. 7. Highly strained compliant optical metamaterials developed by M. Pryce *et al*. [59]. Reprinted (adapted) with permission from [59]. Copyright (2010) American Chemical Society."

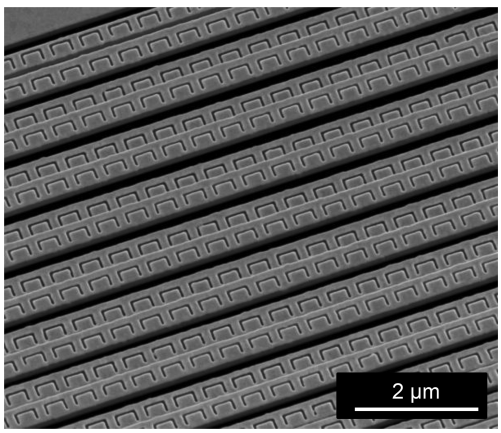

Fig. 8. Thermally-actuated reconfigurable optical metamaterials. More details can be found in Ref. [60]. (Courtesy of Nikolay Zheludev, University of Southampton.)

nant wavelength of the metamaterial was shifted between about 3.5 and 3.9 μm. In general, amount and type of chemicals can be identified by measuring spectra of chemicals using wavelength tuning devices. In addition, PDMS which is used as the material of the flexible substrate has excellent biocompatibility and high optical transparency. Therefore, these results are expected to be applied to biochemical sensors with high sensitivity.

In 2011, Ou *et al*. demonstrated reconfigurable optical metamaterial filters operating at wavelengths around 1200 nm as shown in Fig. 8 [60]. The filters consisted of a pair of reconfigurable and non-reconfigurable bridges with a narrow gap between them. Metamaterial structures were etched on the reconfigurable and non-reconfigurable bridges consisting of multi layers of Au-Si_3N_4 and Au-Si_3N_4-Au, respectively. Since the thermal expansion coefficient of gold is five-times higher than that of silicon nitride, the bridge of the Au-Si_3N_4 layer was bent by a change of temperature and the gap varied. Optical spectra were changed by bending the reconfigurable bridges. At

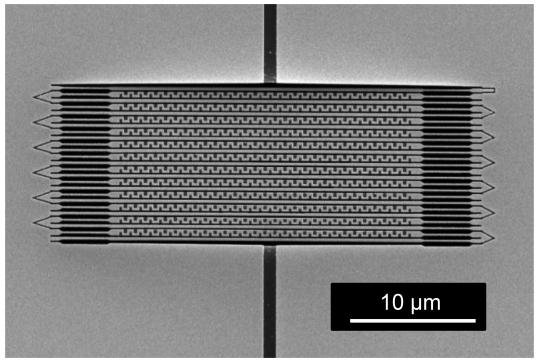

Fig. 9. Electrostatically-actuated reconfigurable optical metamaterials. More details can be found in Ref. [61]. (Courtesy of Nikolay Zheludev, University of Southampton.)

wavelengths of 1180, 1435, and 1735 nm, relative transmittance changes of 37%, 38%, and 51%, respectively, were achieved.

In 2013, Ou *et al*. reported electromechanically tunable metamaterials operating at wavelengths around 1200 nm as shown in Fig. 9 [61]. The metamaterial consisted of a pair of wire and meander structures with a narrow gap between them, which also played a role in the electrodes of electrostatic actuators. By controlling the gap, optical coupling efficiency was tuned and optical characteristics were changed. Transmittance was modulated by about 5% around wavelengths of 1100 and 1300 nm, and reflectance was modulated by up to 8% around 1500 nm. It is notable that a wavelength around 1100 nm is the shortest wavelength as an operating wavelength of reconfigurable optical metamaterials reported so far. When more than 3 V of voltage was applied, the meander structures stuck to the wire structures. Transmittance change of 250% and reflectance change of 110% were achieved at wavelengths around 1200 and 1600 nm, respectively. Large changes of transmittance and reflectance were observed, while the structures could not return from OFF to ON states due to the sticking, which is an issue to be solved.

IV. Points to Be Considered for a Micromachining Process of Optical Metamaterials

In this section, some points to be considered for a micromachining process of optical metamaterials, especially the influence of fabrication errors and substrate materials on optical characteristics, are discussed using Ag and Au nano-rods as simple dipole resonators.

A. Effect of Fabrication Error

Dimension errors occur in fabrication processes as shown in Table II. Fig. 10 shows schematics of a unit structure of a simulation model to evaluate dimension errors of a dipole resonator with a length (d_y), a thickness of Cr (t_c), a thickness of Ag (t_m), and a taper angle (θ). The dipole resonator consisting of Ag is formed periodically in x and y directions on an SiO_2 substrate through a Cr layer as an adhesion layer. The width of the dipole resonator is 100 nm. The environmental medium is assumed to be air. E, H, and k represent the electric field, magnetic field, and wave number of incident light, respectively. Light is impinged at

TABLE II
CLASSIFICATION OF DIMENSION ERRORS AND CALCULATION RANGES

Dimension error	Reference value	Calculation range
Length (d_y)	195 nm (Dipole resonator)	150–250 nm
Thickness of Cr (t_c)	1 nm	0–10 nm
Thickness of Ag (t_m)	45 nm	40–50 nm
Taper angle (θ)	0°	0–30°

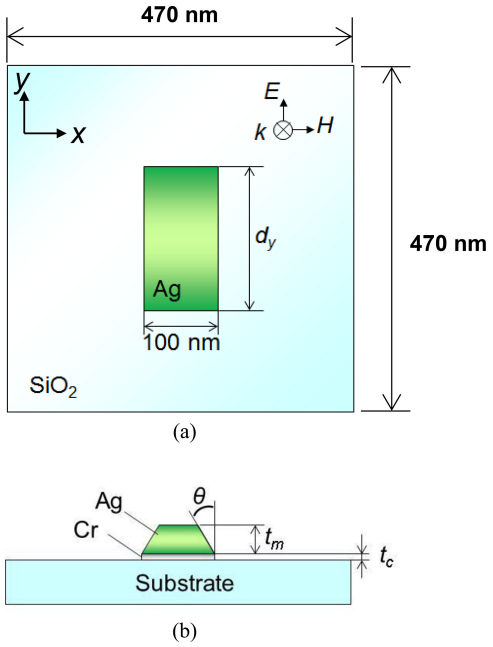

Fig. 10. Schematics of a unit structure of a simulation model to evaluate dimension errors of a dipole resonator with a length (d_y), a thickness of Cr (t_c), a thickness of Ag (t_m), and a taper angle (θ). (a) A top view and (b) a cross-sectional view.

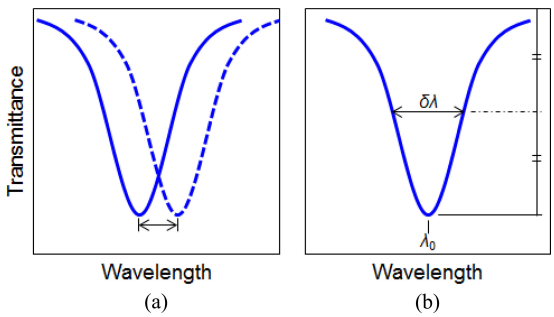

Fig. 11. Definitions of (a) shift of resonant wavelengths and (b) quality factor.

the normal direction from the upper side. The effects of dimension errors were numerically evaluated. Reference values and calculation ranges are also shown in Table II. From calculated optical spectra, changes in resonant wavelengths and quality factors as depicted in Fig. 11 were estimated. The quality factor is expressed as

$$\text{Quality factor} = \frac{\lambda_0}{\delta\lambda}. \tag{6}$$

Transmittance spectra were calculated using rigorous coupled-wave analysis (RCWA), which yields accurate results

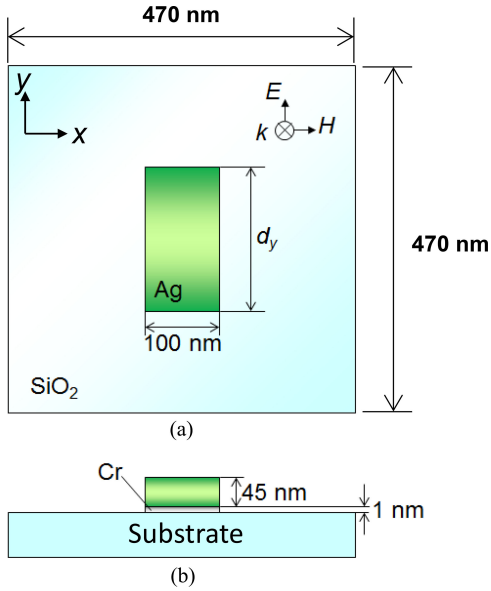

Fig. 12. Schematics of a unit structure of a simulation model to evaluate fabrication error of the length of a dipole resonator. (a) A top view and (b) a cross-sectional view.

using Maxwell's equations in the frequency domain. In the RCWA calculations, a period of 470 nm and the order of Fourier coefficients between −8th and +8th orders were used for each x and y direction. The x and y directions are defined in Fig. 10.

1) Effect of Length: Fig. 12 shows schematics of a unit structure of a simulation model to evaluate dimension errors of the length of a dipole resonator (d_y). The length d_y was changed between 150 and 250 nm.

Fig. 13 shows calculated transmittance spectra and resonant wavelength as a function of d_y. In Fig. 13(a), dips in transmittance, which are caused by dipole resonance, are observed. Also, resonant wavelengths, which are the center wavelengths within the dips, are shifted between 758 and 1000 nm according to the change in d_y as shown in Fig. 13(b). The rate of change in the resonant wavelength with respect to d_y is about 2.5 nm/nm.

2) Effect of Thickness of Chromium: Chromium is required for adhesion layers between metamaterial layers and substrates to improve the adhesion strength. Since chromium has poor plasmonic properties compared with silver and gold, it has the potential to degrade the optical characteristics of metamaterials. The simulation model is similar to that shown in Fig. 12 except that d_y is fixed to 195 nm and the thickness of chromium t_c is changed between 0 and 10 nm. Fig. 14 shows the calculated transmittance spectra as a parameter of t_c. In Fig. 14, optical spectra are drastically changed with a change in t_c. With an increase of t_c, transmittance at resonant wavelengths increases from 4% to 37%, resulting in degradation of optical characteristics. Fig. 15 shows quality factors calculated from the transmittance spectra in Fig. 14. The quality factor gradually decreases with an increase of t_c. At t_c of 0 nm, a quality factor of 6.1 is obtained. At t_c of 10 nm, on the other hand, the quality factor decreases to 2.5. Metamaterials with high quality factors can be obtained by using thin chromium layers.

3) Effect of Thickness of Silver: Although layer thicknesses can be precisely controlled using a crystal oscillator in a depo-

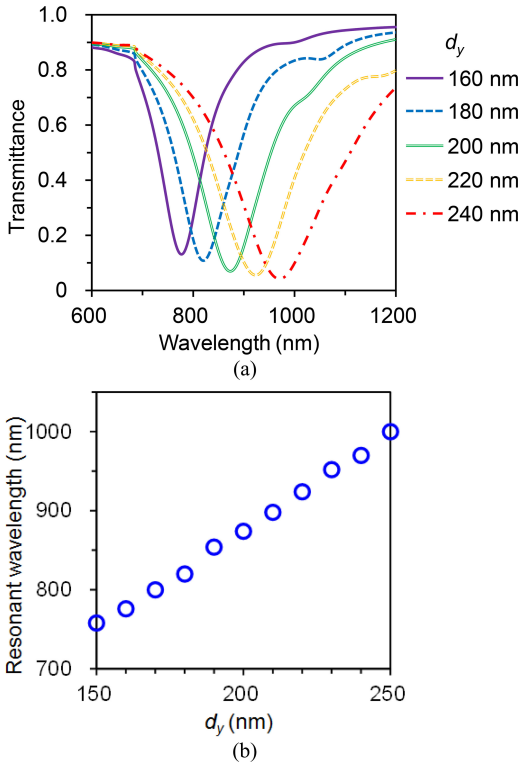

Fig. 13. Calculated (a) transmittance spectra and (b) resonant wavelength as a function of d_y.

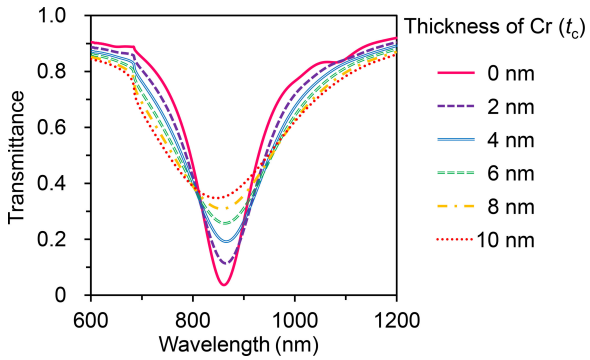

Fig. 14. Calculated transmittance spectra as a parameter of t_c.

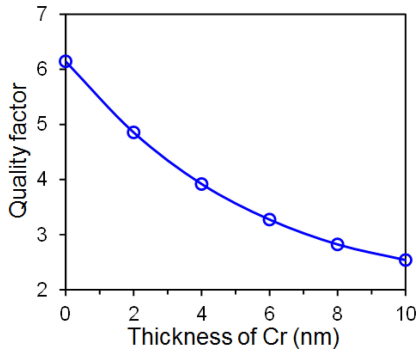

Fig. 15. Calculated quality factor as a function of t_c.

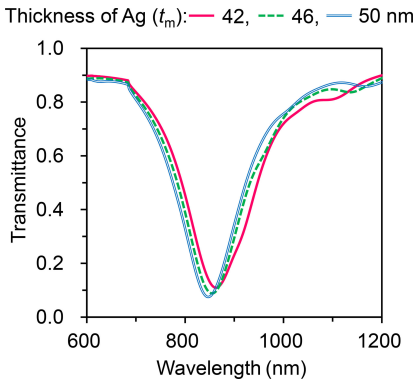

Fig. 16. Calculated transmittance spectra as a parameter of t_m.

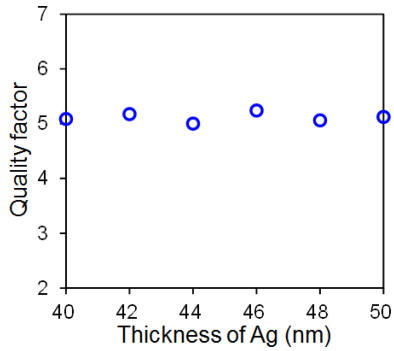

Fig. 17. Calculated quality factor as a function of t_m.

sition process, some errors may occur. In calculations, optical characteristics of the dipole resonator with a thickness of silver t_m between 42 and 50 nm were evaluated. The simulation model is similar to that shown in Fig. 12 except that d_y is fixed to 195 nm and t_m is changed between 42 and 50 nm.Fig. 16 shows the calculated transmittance spectra of the dipole resonator as a function of t_m. It can be seen that there is almost no change in transmittance spectra with change in t_m. Fig. 17 shows the quality factor calculated from the transmittance spectra in Fig. 16. The quality factor is almost unchanged. In this calculation range, the optical characteristics are not greatly affected by the thickness of silver.

4) Effect of Taper Angle: In an etching process, it is difficult to fabricate metamaterial structures with perfectly vertical walls for several reasons such as degradation of mask patterns, surface charge distribution along micro-structured surfaces, and redeposition of etched materials. Thus, a tapered cross section in a microstructure is easily formed. Fig. 18 shows the calculated transmittance spectra of the dipole resonator as a function of taper angle θ between 0 and 30°. The simulation model is similar to that shown in Fig. 12 except that d_y is fixed to 195 nm and the cross section is tapered with an angle θ for the four sides of the dipole resonator as shown in the upper part of Fig. 18. In Fig. 18, the transmittance spectra are changed by change in θ. With an increase of θ, transmittance at resonant wavelengths increases from 8% to 28%, resulting in degradation of optical characteristics. Fig. 19 shows the quality factor as a function of θ calculated from the transmittance spectra in Fig. 18. The quality factor is almost unchanged with an increase of θ. However, since the transmittance spectra are clearly degraded at a large taper angle as can be seen in Fig. 18, the taper angle should

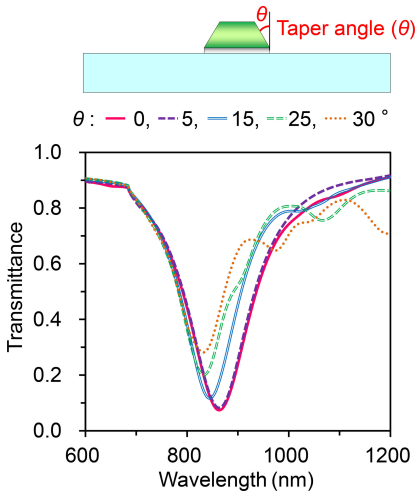

Fig. 18. Calculated transmittance spectra with several taper angles.

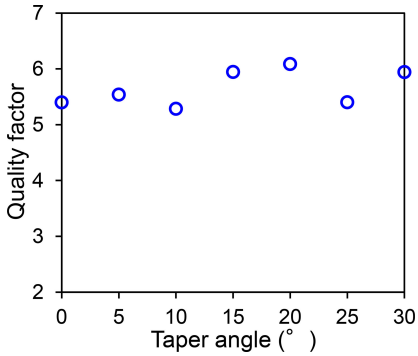

Fig. 19. Calculated quality factor as a function of θ.

be smaller in order to obtain sharp transmittance spectra of the dipole resonators.

Due to etching process or lift-off processes, the corners of the rods that constitute dipole resonators might be rounded. The rods with rounded configurations generate broad and weak resonant spectral responses. In addition, a resonant wavelength is shifted according to the curvature of the corner because the effective-length-change of the rod is caused by a change in the effective refractive index in the vicinity of the corner.

B. *Effect of Substrates*

Si and Si_3N_4 are frequently used as materials of the anchor and supporter for MEMS structures because of their mechanical reliability. However, since Si and Si_3N_4 are high-refractive-index materials, they potentially influence optical characteristics in the shift of resonant wavelengths, optical loss, and so on. Influence of substrate material on optical characteristics was evaluated.

Fig. 20 shows schematics of a unit structure of the simulation model to evaluate the influence of substrate materials. A dipole resonator consisting of Au is formed periodically in x and y directions on a substrate. In the RCWA calculations, a period of 400 nm and the order of Fourier coefficients between $-$8th and $+$8th orders were used for each x and y direction. Air,

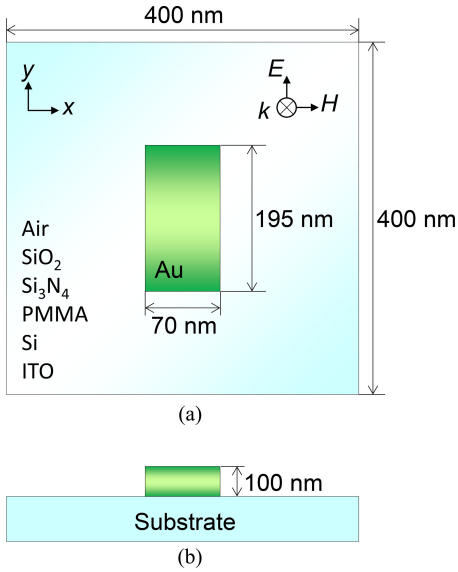

Fig. 20. Schematics of a unit structure of a simulation model to evaluate the influence of substrates. (a) A top view and (b) a cross-sectional view.

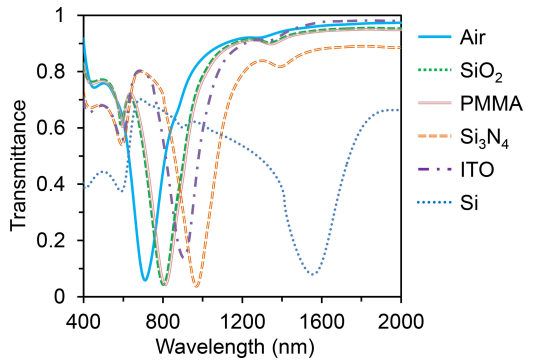

Fig. 21. Calculated transmittance spectra depending on substrate materials.

SiO_2, Si_3N_4, polymethyl methacrylate (PMMA), Si, and indium tin oxide (ITO) were assumed as materials of the substrates. The width, length, and thickness of the dipole resonator were 70, 195, and 100 nm, respectively. The environmental medium was assumed to be air. E, H, and k represent the electric field, magnetic field, and wave number of incident light, respectively. Light was impinged at the normal direction from the upper side.

Fig. 21 shows calculated transmittance spectra with several substrate materials as parameters. In Fig. 21, dips in transmittance spectra, which are caused by the dipole resonance, are observed. The resonant wavelengths differ according to the substrate materials. Although calculated models of metamaterials have the same configuration and dimension, transmittance spectra vary greatly according to materials of substrates. Resonant wavelengths increase with increase of refractive indices of substrates. The resonant wavelengths of air, SiO_2, PMMA, ITO, Si_3N_4, and Si are 710, 802, 812, 906, 968, and 1550 nm, respectively. For ITO and Si, the dip in transmittance at each resonant wavelength is suppressed because these materials have absorption in the calculated wavelength region.

V. Conclusion

MEMS-based reconfigurable metamaterials are candidate technologies for active optical control. In this paper, MEMS-based reconfigurable metamaterials operated in the optical region between visible and near-infrared wavelengths were focused on. Selection of constructional materials for optical metamaterials and typical structures producing excellent magnetic responses at the optical wavelengths were discussed in Section II. In Section III, characteristics of MEMS-based reconfigurable optical metamaterials were revealed and previous studies on MEMS-based reconfigurable optical metamaterials were reviewed. In Section IV, some points to be considered for a micromachining process of optical metamaterials, especially the effects of fabrication errors and substrate materials on optical characteristics, were discussed with results of calculations using Ag and Au nano-rods as simple dipole resonators. The technology of MEMS-based reconfigurable optical metamaterials has taken the first step toward practical use for active optical control. The establishment of fabrication technology and the development of applications for reconfigurable optical metamaterials are important issues. We believe that active optical control using MEMS-based reconfigurable optical metamaterials will be used successfully in practical applications.

References

[1] R. A. Shelby, D. R. Smith, and S. Schultz, "Experimental verification of a negative index of refraction," *Science*, vol. 292, pp. 77–79, 2001.

[2] D. R. Smith, J. B. Pendry, and M. C. K. Wiltshire, "Metamaterials and negative refractive index," *Science*, vol. 305, pp. 788–792, 2004.

[3] S. Zhang *et al.*, "Experimental demonstration of near-infrared negative-index metamaterials," *Phys. Rev. Lett.*, vol. 95, pp. 137404/1–137404/4, 2005.

[4] J. Valentine *et al.*, "Three-dimensional optical metamaterial with a negative refractive index," *Nature*, vol. 455, pp. 376–379, 2008.

[5] X. Wei *et al.*, "A high refractive index metamaterial at visible frequencies formed by stacked cut-wire plasmonic structures," *Appl. Phys. Rev.*, vol. 97, pp. 011904/1–011904/3, 2010.

[6] M. Choi *et al.*, "A terahertz metamaterial with unnaturally high refractive index," *Nature*, vol. 470, pp. 369–373, 2011.

[7] J. B. Pendry, "Negative refraction makes a perfect lens," *Phys. Rev. Lett.*, vol. 85, pp. 3966–3969, 2000.

[8] J. B. Pendry and S. A. Ramakrishna, "Focusing light using negative refraction,"*J. Phys., Condens. Matter*, vol. 15, pp. 6345–6364, 2003.

[9] Z. Liu *et al.*, "Far-field optical hyperlens magnifying sub-diffraction-limited objects," *Science*, vol. 315, p. 1686, 2007.

[10] X. Zhang and Z. Liu, "Superlenses to overcome the diffraction limit," *Nature. Mater.*, vol. 7, pp. 435–441, 2008.

[11] D. Lu and Z. Liu, "Hyperlenses and metalenses for far-field super-resolution imaging," *Nature Commun.*, vol. 3, pp. 1–9, 2012.

[12] D. Schurig *et al.*, "Metamaterial electromagnetic cloak at microwave frequencies," *Science*, vol. 314, pp. 977–980, 2006.

[13] W. Cai, U. K. Chettiar, A. V. Kildishev, and V. M. Shalaev, "Optical cloaking with metamaterials," *Nature Photon.*, vol. 1, pp. 224–227, 2007.

[14] Y. Wang *et al.*, "Metamaterial-plasmonic absorber structure for high efficiency amorphous silicon solar cells," *Nano Lett.*, vol. 12, pp. 440–445, 2012.

[15] M. A. Green and S. Pillai, "Harnessing plasmonics for solar cells," *Nature Photon.*, vol. 6, pp. 130–132, 2012.

[16] L. Liu and S. He, "Near-field optical storage system using a solid immersion lens with a left-handed material slab," *Opt. Exp.*, vol. 12, pp. 4835–4840, 2004.

[17] K. L. Tsakmakidis, A. D. Boardman, and O. Hess, "'Trapped rainbow' storage of light in metamaterials," *Nature*, vol. 450, pp. 397–401, 2007.

[18] T. Chen, S. Li, and H. Sun, "Metamaterials application in sensing," *Sensors*, vol. 12, pp. 2742–2765, 2012.

[19] H. J. Lee, H. S. Lee, H. S. Yoo, and J. G. Yook, "DNA sensing using split-ring resonator alone at microwave regime," *J. Appl. Phys.*, vol. 108, pp. 014908/1–014908/6, 2010.

[20] D. Christian and H. B. Peter, "Frequency selective surfaces for high sensitivity terahertz sensing," *Appl. Phys. Lett.*, vol. 91, pp. 184102/1–184102/3, 2008.

[21] A. V. Kabashin *et al.*, "Plasmonic nanorod metamaterials for biosensing," *Nature Mater.*, vol. 8, pp. 867–871, 2009.

[22] I. A. I. Al-Naib, C. Jansen, and M. Koch, "Thin-film sensing with planar asymmetric metamaterial resonators," *Appl. Phys. Lett.*, vol. 93, pp. 083507/1–083507/3, 2008.

[23] J. F. O'Hara *et al.*, "Thin-film sensing with planar terahertz metamaterials: Sensitivity and limitations," *Opt. Exp.*, vol. 16, pp. 1786–1795, 2008.

[24] Y. T. Chang *et al.*, "A multi-functional plasmonic biosensor," *Opt. Exp.*, vol. 18, pp. 9561–9569, 2010.

[25] R. Melik, E. Unal, N. K. Perkgoz, C. Puttlitz, and H. V. Demir, "Metamaterial based telemetric strain sensing in different materials," *Opt. Exp.*, vol. 18, pp. 5000–5007, 2010.

[26] R. Melik *et al.*, "Flexible metamaterials for wireless strain sensing," *Appl. Phys. Lett.*, vol. 95, pp. 181105/1–181105/3, 2009.

[27] A. J. Ward and J. B. Pendry, "Refraction and geometry in Maxwell's equations," *J. Mod. Opt.*, vol. 43, pp. 773–793, 1996.

[28] M. Rahm *et al.*, "Design of electromagnetic cloaks and concentrators using form-invariant coordinate transformations of Maxwell's equations," *Photon. Nanostruct. Fundam. Appl.*, vol. 6, pp. 87–95, 2008.

[29] J. B. Pendry, D. Schurig, and D. R. Smith, "Controlling electromagnetic fields," *Science*, vol. 312, pp. 1780–1782, 2006.

[30] W. X. Jiang *et al.*, "Design of arbitrarily shaped concentrators based on conformally optical transformation of nonuniform rational B-spline surfaces," *Appl. Phys. Lett.*, vol. 92, pp. 264101/1– 264101/3, 2008.

[31] W. X. Jiang *et al.*, "Arbitrary bending of electromagnetic waves using realizable inhomogeneous and anisotropic materials," *Phys. Rev. E*, vol. 78, pp. 066607/1–066607/4, 2008.

[32] N. I. Zheludev and Y. S. Kivshar, "From metamaterials to metadevices," *Nature Mater.*, vol. 11, pp. 917–924, 2012.

[33] L. Billings, "Exotic optics: Metamaterial world," *Nature*, vol. 500, pp. 138–140, 2013.

[34] A. Q. Liu, W. M. Zhu, D. P. Tsai, and N. I. Zheludev, "Micromachined tunable metamaterials: A review," *J. Opt.*, vol. 14, pp. 114009/1–114009/8, 2012.

[35] H.-T. Chen *et al.*, "Active terahertz metamaterial devices," *Nature*, vol. 444, pp. 597–600, 2006.

[36] H.-T. Chen *et al.*, "A metamaterial solid-state terahertz phase modulator," *Nature Photon.*, vol. 3, pp. 148–151, 2009.

[37] D. Shrekenhamer *et al.*, "High speed terahertz modulation from metamaterials with embedded high electron mobility transistors," *Opt. Exp.*, vol. 19, pp. 9968–9975, 2011.

[38] L. Ju *et al.*, "Graphene plasmonics for tunable terahertz metamaterials," *Nature Nanotechnol.*, vol. 6, pp. 630–634, 2011.

[39] S. H. Lee *et al.*, "Switching terahertz waves with gate-controlled active graphene metamaterials," *Nature Mater.*, vol. 11, pp. 936–941, 2012.

[40] Y. Urzhumov *et al.*, "Electronically reconfigurable metal-on-silicon metamaterial," *Phys. Rev. B*, vol. 86, pp. 075112/1–075112/10, 2012.

[41] J. Han, A. Lakhtakia, and C.-W. Qiu, "Terahertz metamaterials with semiconductor split-ring resonators for magnetostatic tunability," *Opt. Exp.*, vol. 16, pp. 14390–14396, 2008.

[42] H.-T. Chen *et al.*, "Experimental demonstration of frequency-agile terahertz metamaterials," *Nature Photon.*, vol. 2, pp. 295–298, 2008.

[43] D. R. Chowdhury *et al.*, "Dynamically reconfigurable terahertz metamaterial through photo-doped semiconductor," *Appl. Phys. Lett.*, vol. 99, pp. 231101/1–231101/3, 2011.

[44] N.-H. Shen *et al.*, "Optically implemented broadband blueshift switch in the terahertz regime," *Phys. Rev. Lett.*, vol. 106, pp. 037403/1–037403/4, 2011.

[45] J. Gu *et al.*, "Active control of electromagnetically induced transparency analogue in terahertz metamaterials," *Nat. Commun.*, vol. 3, pp. 1151/1–1151/6, 2012.

[46] T. Driscoll *et al.*, "Dynamic tuning of an infrared hybrid-metamaterial resonance using vanadium dioxide," *Appl. Phys. Lett.*, vol. 93, pp. 024101/1–024101/3, 2008.

[47] T. Driscoll *et al.*, "Memory metamaterials," *Science*, vol. 325, pp. 1518–1521, 2009.

[48] H. Němec *et al.*, "Tunable terahertz metamaterials with negative permeability," *Phys. Rev. B*, vol. 79, pp. 241108/1–241108/4, 2009.
[49] M. J. Dicken *et al.*, "Frequency tunable near-infrared metamaterials based on VO2 phase transition," *Opt. Exp.*, vol. 17, pp. 18330–18339, 2009.
[50] D. H. Werner *et al.*, "Liquid crystal clad near-infrared metamaterials with tunable negative-zero-positive refractive indices," *Opt. Exp.*, vol. 15, pp. 3342–3347, 2007.
[51] D. Shrekenhamer, W.-C. Chen, and W. J. Padilla, "Liquid crystal tunable metamaterial absorber," *Phys. Rev. Lett.*, vol. 110, pp. 177403/1–177403/5, 2013.
[52] W. M. Zhu *et al.*, "Switchable magnetic metamaterials using micromachining processes," *Adv. Mat.*, vol. 23, pp. 1792–1796, 2011.
[53] Y. H. Fu *et al.*, "A Micromachined reconfigurable metamaterial via reconfiguration of asymmetric split-ring resonators," *Adv. Mat.*, vol. 21, pp. 3589–3594, 2011.
[54] E. Ekmekci *et al.*, "Frequency tunable terahertz metamaterials using broadside coupled split-ring resonators," *Phys. Rev. B*, vol. 83, pp. 193103/1–193103/4, 2011.
[55] H. Tao *et al.*, "MEMS based structurally tunable metamaterials at terahertz frequencies," *J. Infrared Millim. Terahertz Waves*, vol. 32, pp. 580–595, 2011.
[56] W. Zhang *et al.*, "Micromachined switchable metamaterial with dual resonance," *Appl. Phys. Lett.*, vol. 101, pp. 151902/1–151902/4, 2012.
[57] W. M. Zhu *et al.*, "Microelectromechanical Maltese-cross metamaterial with tunable terahertz anisotropy," *Nat. Commun.*, vol. 3, pp. 1274/1–1274/6, 2012.
[58] Z. Han *et al.*, "MEMS reconfigurable metamaterial for terahertz switchable filter and modulator," *Opt. Exp.*, vol. 22, pp. 21326–21339, 2014.
[59] I. M. Pryce *et al.*, "Highly strained compliant optical metamaterials with large frequency tunability," *Nano Lett.*, vol. 10, pp. 4222–4227, 2010.
[60] J. Y. Ou, E. Plum, L. Jiang, and N. I. Zheludev, "Reconfigurable photonic metamaterials," *Nano Lett.*, vol. 11, pp. 2142–2144, 2011.
[61] J.-Y. Ou, E. Plum, J. Zhang, and N. I. Zheludev, "An electromechanically reconfigurable plasmonic metamaterial operating in the near-infrared," *Nat. Nanotechnol.*, vol. 8, pp. 252–255, 2013.
[62] W. Cai and V. Shalaev, "Optical properties of metal-dielectric composites," in *Optical Metamaterials: Fundamentals and Applications*, New York, NY, USA: Springer, 2010, ch. 2, pp. 11–37.
[63] C. J. Powell, "Analysis of optical and inelastic-electronscattering data II. Application to Al," *J. Opt. Soc. Amer.*, vol. 60, pp. 78–93, 1970.
[64] M. Erman *et al.*, "Optical properties and damage analysis of GaAs single crystals partly amorphized by ion implantation," *J. Appl. Phys.*, vol. 56, pp. 2664–2671, 1984.
[65] R. Brendel and D. Bormann, "An infrared dielectric function model for amorphous solids," *J. Appl. Phys.*, vol. 71, pp. 1–6, 1992.
[66] D. Rakić, A. B. Djurišić, J. M. Elazar, and M. L. Majewski, "Optical properties of metallic films for vertical-cavity optoelectronic devices," *Appl. Opt.*, vol. 37, pp. 5271–5283, 1998.
[67] J. Zhou *et al.*, "Saturation of the magnetic response of split-ring resonators at optical frequencies," *Phys. Rev. Lett.*, vol. 95, pp. 223902/1–223902/4, 2005.
[68] A. Ishikawa, T. Tanaka, and S. Kawata, "Negative magnetic permeability in the visible light region," *Phys. Rev. Lett.*, vol. 95, p. 237401/1–237401/4, 2005.
[69] S. Linden *et al.*, "Photonic metamaterials: Magnetism at optical frequencies," *IEEE J. Sel. Topics Quantum Electron.*, vol. 12, no. 6, pt. 1, pp. 1097–1105, Nov./Dec. 2006.
[70] M. W. Klein, C. Enkrich, M. Wegener, and S. Linden, "Second-harmonic generation from magnetic metamaterials," *Science*, vol. 313, pp. 502–504, 2006.
[71] N. Liu *et al.*, "Three-dimensional photonic metamaterials at optical frequencies," *Nature Mater.*, vol. 7, pp. 31–37, 2008.
[72] X. Xu *et al.*, "Flexible visible-infrared metamaterials and their applications in highly sensitive chemical and biological sensing," *Nano Lett.*, vol. 11, pp. 3232–3238, 2011.
[73] S. Xiao *et al.*, "Loss-free and active optical negative-index metamaterials," *Nature*, vol. 466, pp. 735–738, 2010.
[74] C. Menzel *et al.*, "Validity of effective material parameters for optical fishnet metamaterials," *Phys. Rev. B*, vol. 81, pp. 035320/1–035320/5, 2010.
[75] F. Hao *et al.*, "Symmetry breaking in plasmonic nanocavities: Subradiant LSPR sensing and a tunable Fano resonance," *Nano Lett.*, vol. 8, pp. 3983–3988, 2008.
[76] B. Luk'yanchuk *et al.*, "The Fano resonance in plasmonic nanostructures and metamaterials," *Nature Mater.*, vol. 9, pp. 707–715, 2010.
[77] H. Liu *et al.*, "Linear and nonlinear Fano resonance on two-dimensional magnetic metamaterials," *Phys. Rev. B*, vol. 84, pp. 235437/1–235437/6, 2011.
[78] L. Shao *et al.*, "Distinct plasmonic manifestation on gold nanorods induced by the spatial perturbation of small gold nanospheres," *Nano Lett.*, vol. 12, pp. 1424–1430, 2012.
[79] Y. Moritake, Y. Kanamori, and K. Hane, "Experimental demonstration of sharp Fano resonance in optical metamaterials composed of asymmetric double bars," *Opt. Lett.*, vol. 39, pp. 4057–4060, 2014.
[80] S. Zhang *et al.*, "Plasmon-induced transparency in metamaterials," *Phys. Rev. Lett.*, vol. 101, pp. 047401/1–047401/4, 2008.
[81] N. Liu *et al.*, "Plasmonic analogue of electromagnetically induced transparency at the Drude damping limit," *Nature Mater.*, vol. 8, pp. 758–762, 2009.
[82] N. Varellen *et al.*, "Fano resonances in individual coherent plasmonic nanocavities," *Nano Lett.*, vol. 9, pp. 1663–1667, 2009.
[83] J. Zhang *et al.*, "Electromagnetically induced transparency in metamaterials at near-infrared frequency," *Opt. Exp.*, vol. 18, pp. 17187–17192, 2010.
[84] N. Liu *et al.*, "Planar metamaterial analogue of electromagnetically induced transparency for plasmonic sensing," *Nano Lett.*, vol. 10, pp. 1103–1107, 2010.
[85] K. O'Brien *et al.*, "Reflective interferometry for optical metamaterial phase measurements," *Opt. Lett.*, vol. 37, pp. 4089–4091, 2012.
[86] A. E. Çetin *et al.*, "Plasmon induced transparency in cascaded π-shaped metamaterials," *Opt. Exp.*, vol. 19, pp. 22607–22618, 2011.
[87] R. Hokari, Y. Kanamori, and K. Hane, "Fabrication of planar metamaterials with sharp and strong electromagnetically induced transparency-like characteristics at wavelengths around 820 nm," *J. Opt. Soc. Amer. B*, vol. 31, pp. 1000–1005, 2014.
[88] R. Hokari, Y. Kanamori, and K. Hane, "Comparison of electromagnetically induced transparency between silver, gold, and aluminum metamaterials at visible wavelengths," *Opt. Exp.*, vol. 22, pp. 3526–3537, 2014.

Yoshiaki Kanamori received the M.S. and Dr.Eng. degrees from Tohoku University, Sendai, Japan, in 1998 and 2001, respectively.

From 1998 to 2001, he was a Research Fellow of the Japan Society for the Promotion of Science. From 2001 to 2007, he was a Research Associate with the Graduate School of Engineering, Tohoku University. From 2003 to 2004, he was a Postdoctoral Researcher with the Laboratory for Photonics and Nanostructures, Centre National de la Recherche Scientifique, Paris, France. Since 2007, he has been an Associate Professor with the Department of Nanomechanics, Tohoku University. He is currently engaged in research and development of nanophotonics and optical MEMS.

Ryohei Hokari received the M.S. and Dr.Eng. degrees from Tohoku University, Sendai Japan, in 2010 and 2014, respectively.

He is currently a Research Fellow of the Japan Society for the Promotion of Science.

Kazuhiro Hane received the M.S. and Dr.Eng. degrees from Nagoya University, Nagoya, Japan, in 1980 and in 1983, respectively.

From 1983 to 1994, he was a Member of the Faculty of the Department of Electrical Engineering, Nagoya University. From 1985 to 1986, he was a Visiting Researcher of the National Research Council of Canada. Since 1994, he has been a Professor with the Department of Nanomechanics, Tohoku University, Sendai, Japan, where he is currently engaged in research and development of optical microsensors and optical MEMS.